



## New evidence for alpha clustering structure in the ground state band of $^{212}\text{Po}$



Ma. von Tresckow<sup>a,\*</sup>, M. Rudigier<sup>a</sup>, T.M. Shneidman<sup>b</sup>, Th. Kröll<sup>a</sup>, M. Boromiza<sup>c</sup>, C. Clisu<sup>c</sup>, C. Costache<sup>c</sup>, D. Filipescu<sup>c</sup>, N.M. Florea<sup>c</sup>, I. Gheorghe<sup>c</sup>, K. Gladnishki<sup>d</sup>, A. Ionescu<sup>c</sup>, D. Kocheva<sup>d</sup>, R. Lică<sup>c</sup>, N. Mărginean<sup>c</sup>, R. Mărginean<sup>c</sup>, K.R. Mashtakov<sup>e,f,h</sup>, C. Mihai<sup>c</sup>, R.E. Mihai<sup>c</sup>, A. Negret<sup>c</sup>, C.R. Nita<sup>c</sup>, A. Olacel<sup>c</sup>, A. Oprea<sup>c</sup>, S. Pascu<sup>c</sup>, G. Rainovski<sup>d</sup>, T. Sava<sup>c</sup>, M. Scheck<sup>e,f</sup>, P. Spagnoletti<sup>e,f,g</sup>, C. Sotty<sup>c</sup>, L. Stan<sup>c</sup>, I. Stiru<sup>c</sup>, S. Toma<sup>c</sup>, A. Turturică<sup>c</sup>, S. Ujenuc<sup>c</sup>

<sup>a</sup> Institut für Kernphysik, Technische Universität Darmstadt, Schlossgartenstrasse 9, 64289, Darmstadt, Germany

<sup>b</sup> Joint Institute for Nuclear Research, Dubna 141980, Russia

<sup>c</sup> Horia Hulubei National Institute of Physics and Nuclear Engineering (IFIN-HH), R-077125 Bucharest, Romania

<sup>d</sup> Faculty of Physics, St. Kliment Ohridski University of Sofia, 1164 Sofia, Bulgaria

<sup>e</sup> University of the West of Scotland, PA1 2BE Paisley, United Kingdom

<sup>f</sup> SUPA, Glasgow G12 8QQ, United Kingdom

<sup>g</sup> Simon Fraser University, 8888 University Drive, Burnaby, B.C., V5A 1S6, Canada

<sup>h</sup> University of Guelph, 50 Stone Road E., Guelph, Ontario, N1G 2W1, Canada

### ARTICLE INFO

#### Article history:

Received 15 July 2021

Received in revised form 31 August 2021

Accepted 2 September 2021

Available online 6 September 2021

Editor: D.F. Geesaman

#### Keywords:

$^{212}\text{Po}$

Lifetime measurement

$\alpha$ -clustering in nuclear

Centroid shift method

### ABSTRACT

Half-lives of the low-lying yrast states of  $^{212}\text{Po}$  have been measured using the delayed coincidence fast-timing method. We report on the first measurement of the  $4_1^+$  half-life, as well as a new measurement of the  $6_1^+$  half-life with improved accuracy compared to previous studies. The extracted lifetime of the  $4_1^+$  and  $6_1^+$  state have been determined to be 100(14) ps and 1.66(28) ns respectively. With these measurements, precise values are now available for the reduced transition strengths  $B(E2)$  of all ground state band levels in  $^{212}\text{Po}$  up to the first  $8^+$  state, in particular  $B(E2; 4_1^+ \rightarrow 2_1^+) = 9.4(13)$  W.u. and  $B(E2; 6_1^+ \rightarrow 4_1^+) = 8.7(15)$  W.u. Comparison of the new available data with an  $\alpha$ -clustering model calculation provides evidence that the inclusion of the  $\alpha$ -cluster degree of freedom significantly improves agreement with experimental data compared to earlier shell model calculations.

© 2021 The Authors. Published by Elsevier B.V. This is an open access article under the CC BY license (<http://creativecommons.org/licenses/by/4.0/>). Funded by SCOAP<sup>3</sup>.

### 1. Introduction

The isotope  $^{212}\text{Po}$  has two protons and neutrons outside the doubly-magic nucleus  $^{208}\text{Pb}$ . Therefore, it can be expected that its dynamics and structure can be described by the nuclear shell model [1]. While the energy of the excited states can be well reproduced within the shell model, several measured properties of this isotope cannot be described by this approach. One of these properties is the large  $\alpha$ -decay width of the short-lived ground state which indicates a high probability of preformation of an  $\alpha$  particle inside the nucleus [2]. This has motivated the description of  $^{212}\text{Po}$  by strongly mixing shell-model and  $\alpha$ -cluster configurations [3–5] which can reproduce the  $\alpha$ -decay width of the ground

state fairly well. Another evidence for the  $\alpha$ -clustering in  $^{212}\text{Po}$  is the observation of enhanced E1 transitions from several states at excitation energies above 1.7 MeV with non-natural parity [6,7]. This is interpreted to be due to the presence of large  $\alpha$ -cluster components in the wave functions of these states.

Less clear is the tendency of the  $B(E2)$  values for the decays of the low-lying yrast states where the transition strength of the decay of the  $4_1^+$  state is unknown yet. The decay of the  $2_1^+$  state has an absolute transition strength  $B(E2)$  value of 2.6(3) W.u. [8] and is thus overestimated by  $\alpha$ -clustering models (7.41 W.u. [4],  $\sim 4.57$  W.u. [5], 9.2 W.u. [9]). In contrast to the  $2_1^+$  state, the experimental  $B(E2)$  values of the decay of the  $6_1^+$  and  $8_1^+$  state (13.2<sup>+4.9</sup><sub>-2.9</sub> W.u. and 4.6(1) W.u. respectively [10]) have higher collectivity and are more consistent with  $\alpha$ -clustering models. The  $B(E2; 6_1^+ \rightarrow 4_1^+)$  value is predicted within the  $\alpha$ -clustering models to be 10.62 W.u. [4],  $\sim 6.6$  W.u. [5] and 14.4 W.u. [9]. The decay of

\* Corresponding author.

E-mail address: [mtresckow@ikp.tu-darmstadt.de](mailto:mtresckow@ikp.tu-darmstadt.de) (Ma. von Tresckow).

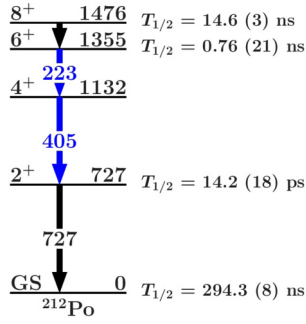


**Fig. 1.** Partial level scheme of the low-lying yrast states of  $^{212}\text{Po}$ . The major coincidence to determine the lifetime of the  $4_1^+$  state applying the centroid shift method is marked in blue. The half-lives of the others are taken from Ref. [10].

the  $8_1^+$  state in this model has an absolute transition strength of 10.04 W.u.[4],  $\sim 6.1$  W.u. [5] and 5.8 W.u. [9].

The low collectivity of the  $2_1^+$  state implies that the structure of this state could be described within the framework of nuclear shell model. Indeed, an existing shell model calculation yields a value of  $B(E2; 2_1^+ \rightarrow 0_1^+) = 3.6$  W.u. (SM2 – gh from Ref. [8]), which fits the experimental value better than  $\alpha$ -clustering model predictions. However, the predictions of the shell model calculation are too low to reproduce the experimental  $B(E2; 6_1^+ \rightarrow 4_1^+)$  and  $B(E2; 8_1^+ \rightarrow 6_1^+)$  values ([2.4, 0.8] W.u., respectively). Recent shell model calculation uses the new effective interaction H208 derived from CD-Bonn nucleon-nucleon interaction and different proton and neutron charges due to the neutron dominance in the  $2_1^+$  state [11]. This calculation predicts enhanced  $B(E2)$  values for the decays of the low-lying yrast states [11]. The  $B(E2)$  values of the decay of the  $6_1^+$  and  $8_1^+$  state ([4.42, 2.34] W.u. [11]) are getting closer to the experimental  $B(E2)$  values but are still too small.

Reported experimental  $\alpha$ -branching ratios for the  $6_1^+$  and  $8_1^+$  states are contradicting. The large values of 71% and 42%, respectively, from Ref. [12], which are adopted by Ref. [13], lead to smaller experimental  $B(E2)$  values of [3.9(11), 2.30(9)] W.u. [13] but other measurements [7,14] have concluded on smaller  $\alpha$ -branching ratios around 3% for both states. These values are now adopted in the recent compilation [10].

Therefore the missing  $B(E2; 4_1^+ \rightarrow 2_1^+)$  value is an important puzzle piece in the discussion of the  $B(E2)$  values and can allow for a deeper insight into the competition between both models in this nucleus. The missing  $B(E2)$  value can be deduced if the lifetime of the  $4_1^+$  state is measured.

Due to the short lifetime of the ground state, the experimental access to the isotope  $^{212}\text{Po}$  is difficult and was successfully done via light-ion-induced transfer reaction on a  $^{208}\text{Pb}$  target [8,15,16]. These reactions have several channels and the separation of the events belonging to the population of low-lying yrast states of  $^{212}\text{Po}$ , shown in Fig. 1, is an experimental challenge. One of the solutions available, used also in Ref. [8], is the use of an additional particle detector setup select the  $\alpha$ -transfer channel by detecting the reaction product. However, the expected lifetime of the  $4_1^+$  state may be too long for applying the Recoils distance method. An alternative approach is the centroid shift method for delayed coincidence fast timing, which is very well suited for lifetimes in the expected range. To determine the missing transition probability, this article reports the first lifetime determination of this state, using a fast-timing setup combined with a particle detector array.

## 2. Experimental setup

To populate excited states in  $^{212}\text{Po}$  the alpha transfer reaction  $^{208}\text{Pb}(^{10}\text{B}, ^6\text{Li})^{212}\text{Po}$  was used at a  $^{10}\text{B}$  beam energy of 51 MeV, which is around the Coulomb barrier. The ion beam from

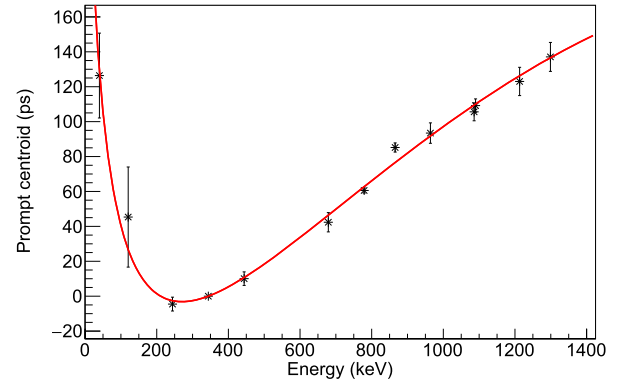


**Fig. 2.** Prompt response time walk  $C^P(E_\gamma, 344 \text{ keV})$  relative to the reference Decay energy  $E_{d,ref} = 344 \text{ keV}$ . The fit function to describing the time walk is shown in red. Between 200 keV and 1300 keV we assume an uncertainty of 7 ps for the calibration. Below 200 keV the uncertainty is less precise. We estimate 30 ps at energy 121 keV.

the Bucharest FN Tandem Accelerator [17] was impinged on a 9.65 mg/cm<sup>2</sup> target of enriched  $^{208}\text{Pb}$  (99.14%). The strongest additional reaction channels are the fusion-evaporation to  $^{214,215}\text{Fr}$ ,  $^{211,212}\text{At}$ , and the one proton transfer leading to  $^{209}\text{Bi}$ .

The experiment was performed with the ROSPHERE array [18] at the Horia Hulubei National Institute for R&D in Physics and Nuclear Engineering (IFIN-HH) in Magurele, Romania. The array consisted of 15 high purity Germanium detectors (HPGe) with active anti-Compton shields and 10 lead shielded  $\text{LaBr}_3(\text{Ce})$  fast-timing scintillator detectors arranged in five rings. The HPGe detectors were placed in ring number 1 (37 degree with respect to the beam axis), 3 (90 degree), and 5 (143 degree) and the  $\text{LaBr}_3(\text{Ce})$  detectors were placed in rings 2 (70 degree) and 4 (110 degree). The cylindrical 2 inch x 2 inch (length x diameter)  $\text{LaBr}_3(\text{Ce})$  crystals have a  $\gamma$ - $\gamma$  coincidence time resolution of 309(1) ps (FWHM) measured with the 1173 keV – 1332 keV coincidences from a  $^{60}\text{Co}$  source. During this experimental campaign, ROSPHERE was supplemented by the particle detector array SORCERER [19]. The six Silicon photodiodes cover a polar angle range from 121.7 degree to 163.5 degree with respect to the beam direction [19].

During the ten-day measurement, two trigger conditions were used: (one Si hit AND one  $\text{LaBr}_3(\text{Ce})$  event) OR two clean Ge events. The trigger window of the more important Si- $\text{LaBr}_3(\text{Ce})$  trigger had a size of 200 ns.

## 3. Data analysis and results

For the lifetime analysis, the centroid shift method [20] was applied. This method is based on the delayed time difference distribution of the  $\gamma$ - $\gamma$  coincidence between the transitions populating (*Feeder*) and depopulating (*Decay*) the state of interest. The centroid position  $C$  of this distribution is shifted by the mean lifetime  $\tau$  of the intermediate state with respect to the centroid  $C^P$  of the intrinsic time difference distribution of the setup (prompt response distribution):

$$C(E_f, E_d) = \tau + C^P(E_f, E_d).$$

The centroid  $C^P$  depends on the energies  $E_f$  and  $E_d$  of the coincidence *Feeder* and *Decay* transitions, which results in a prompt response time walk for the  $\text{LaBr}_3(\text{Ce})$  scintillators [21]. The timing (and energy) calibration of the setup was done by a measurement using a  $^{152}\text{Eu}$  source, which provides several calibration points in the energy region between the X-ray energies ( $\sim 40 \text{ keV}$ ) up to 1299 keV. The resulting prompt response time walk curve of this analysis is shown in Fig. 2 and was confirmed by measuring known

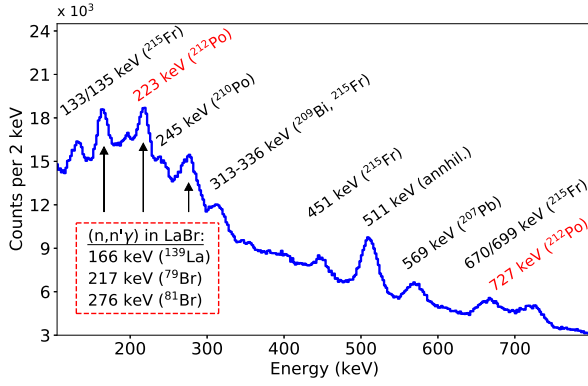


Fig. 3. LaBr<sub>3</sub>(Ce) spectrum of gamma-rays in coincident with the 405-keV transitions recorded in the LaBr<sub>3</sub>(Ce) detectors.

lifetimes in isotopes produced by other reaction channels during the experimental run (<sup>210</sup>Po, <sup>209</sup>Bi, and <sup>207</sup>Pb).

### 3.1. Separation of <sup>212</sup>Po data

Due to the contaminations in the recorded spectra from other reaction channels, shown in Fig. 3, the study of the lifetime of the 4<sub>1</sub><sup>+</sup> state of <sup>212</sup>Po is only possible by applying different gating conditions on the LaBr<sub>3</sub>(Ce) and Silicon timing and energy spectra. Especially the low peak-to-background ratio and the contaminating 217-keV transition, caused by inelastic neutron scattering in the LaBr<sub>3</sub>(Ce) detectors, pose a problem for the lifetime determination because the only usable feeding transition of the 4<sub>1</sub><sup>+</sup> state in this analysis has an energy of 223 keV.

The advantage of this experimental setup is the opportunity to use the coincidence between the  $\gamma$ -rays of <sup>212</sup>Po detected in RO-SPHERE and the <sup>6</sup>Li ejectile from the  $\alpha$ -transfer reaction detected in SORCERER. The ungated, scaled particle-energy spectrum is shown in Fig. 4 (blue). In order to extract from this double-humped spectrum the particle events associated with the  $\alpha$ -transfer reaction, a coincidence with the 727-keV gamma-rays recorded in the HPGe detectors was applied (Fig. 4 red spectrum). All Si events belonging to <sup>212</sup>Po are located in the lower energy bump.

Another gate to separate the <sup>212</sup>Po data was a Si-LaBr<sub>3</sub>(Ce) time difference (SLTD) gate. The SLTD spectrum with a LaBr<sub>3</sub>(Ce) energy gate on the 223 keV - 405 keV coincidence is shown in Fig. 4 and can be separated into three different sections. 1st: The desired events corresponding to the Si-LaBr<sub>3</sub>(Ce) trigger peak at around 3775 ns belong to the scenario where the events are detected in the LaBr<sub>3</sub>(Ce) and Si detector at the same time. This is the *prompt* region. 2nd: If the LaBr<sub>3</sub>(Ce) event was detected first, the corresponding events had a time difference larger than the prompt region (> 3800 ns). The events of this scenario mainly belonged to the de-excitation of <sup>215</sup>Fr and the following detection of the  $\alpha$  particle from the decay of the ground state ( $T_{1/2} = 86(5)$  ns [22]). 3rd: In the opposite scenario for which the Si event was detected first, the SLTD is smaller than the prompt region (< 3760 ns). This scenario appeared e.g. in the population of the isomeric 8<sup>+</sup> state of <sup>212</sup>Po. The <sup>6</sup>Li ejectile was detected first and the  $\gamma$ -rays of the decay cascade from the 8<sub>1</sub><sup>+</sup> state were detected delayed due to the lifetime of the state ( $T_{1/2} = 14.6(8)$  ns [10]). Therefore the lifetime of the 8<sub>1</sub><sup>+</sup> state can be measured using the SLTD distribution and the slope method. In the following analysis a SLTD gate on this slope of the exponential decay of the isomer was used which is marked in light-blue in Fig. 4.

Besides the Si gates, a LaBr<sub>3</sub>(Ce) timing gate was set on the TDC trigger regions, and a Si multiplicity condition was set so that the coincidence event should contain only one event in the Si detectors.

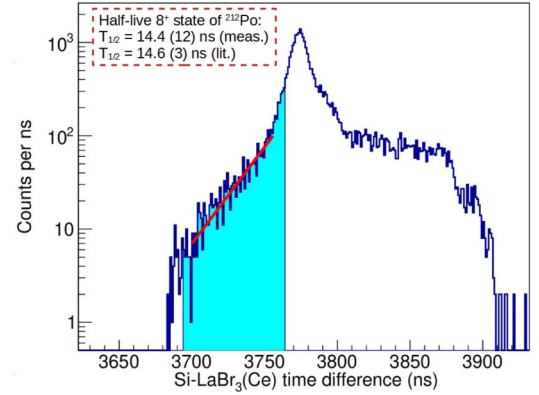
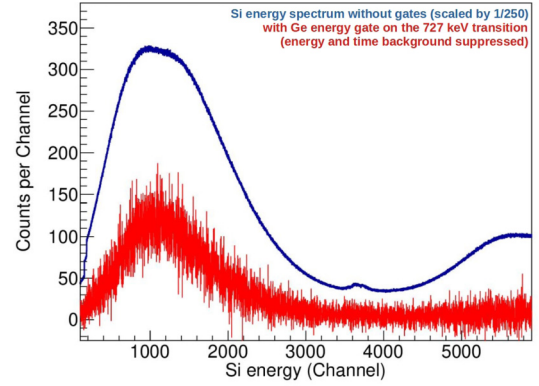


Fig. 4. Top: Show is the ungated (blue) and gated (red) particle-energy spectra as recorded in the Si detectors. For the lower (red) spectrum a gate on the 727-keV transition detected in the HPGe detectors was applied. Bottom: Si-LaBr<sub>3</sub>(Ce) time-difference (SLTD) spectrum with an energy gate on the 223 keV - 405 keV coincidence gate. The SLTD gate is shown in light blue. In red is shown the exponential fit to measure the half-life of the 8<sub>1</sub><sup>+</sup> state of <sup>212</sup>Po using the slope method. The literature value is taken from Ref. [10].

### 3.2. Lifetime determination of the 4<sub>1</sub><sup>+</sup> state

Fig. 5 (a) shows the cleaned coincidence  $\gamma$ -ray spectra with a LaBr<sub>3</sub>(Ce) energy gate on the 405-keV transition (4<sub>1</sub><sup>+</sup>  $\rightarrow$  2<sub>1</sub><sup>+</sup>). The peaks corresponding to the populating 223-keV (6<sub>1</sub><sup>+</sup>  $\rightarrow$  4<sub>1</sub><sup>+</sup>) and 121-keV  $\gamma$ -rays (8<sub>1</sub><sup>+</sup>  $\rightarrow$  6<sub>1</sub><sup>+</sup>) are clearly present. The amount of contaminations is low and peaks belonging to the inelastic neutron scattering in the LaBr<sub>3</sub>(Ce) detectors are completely suppressed by the gates. The peak-to-background ratio of the 223-keV (405-keV) peak has within the later gate sizes a value of 1.79(9) (1.86(11)).

The measured time difference distribution for the determination of the lifetime of the 4<sub>1</sub><sup>+</sup> state is shown in Fig. 5 (c) and has a centroid value of 33(7) ps. An important step in the centroid shift method is the background correction of the centroid value. This correction was done in the present work using an analytical time-correction term described in Ref. [23] and used in different analyses (e.g. [24–26]). In this approach, the corrected centroid position is given by

$$C_{cor} = C_{exp} + \tilde{t}_{cor}.$$

The analytical time-correction term  $\tilde{t}_{cor}$  can be calculated from the centroids of the Compton background at the peak position together with the peak-to-background ratios and the measured centroid value [23]. The centroid of the Compton background at the peak position is interpolated by a polynomial fit on measured centroids in the pure background region (Fig. 5 (a,b)).

Using the Compton background corrected centroid position  $C_{cor} = 93(10)$  ps ( $\tilde{t}_{cor} = 60(7)$  ps), the prompt response centroid

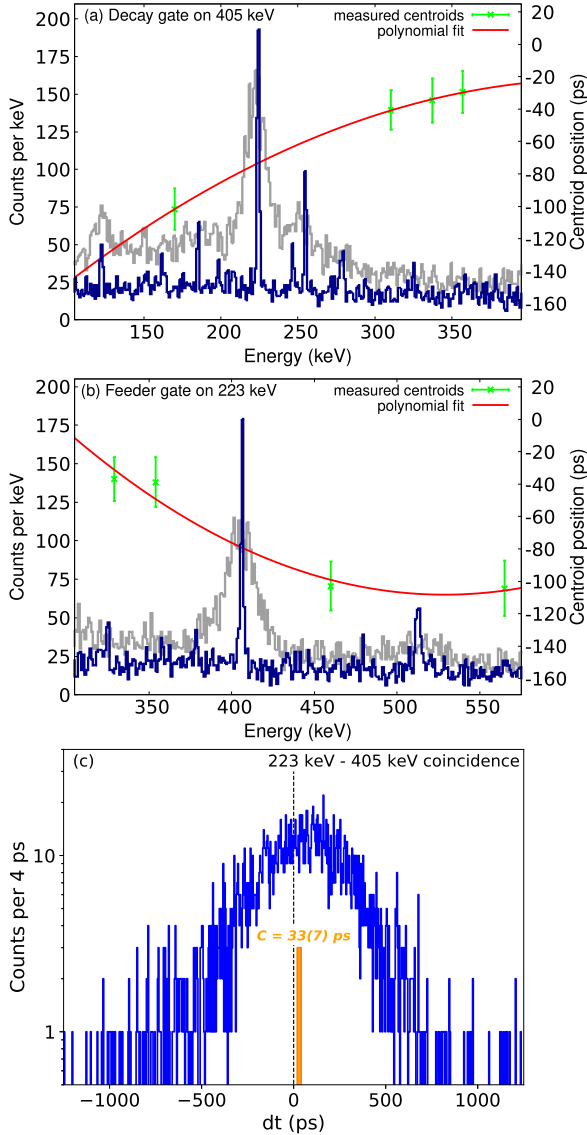


**Fig. 5.** (a) The coincidence LaBr<sub>3</sub>(Ce) (grey) and HPGe (blue) spectra with a LaBr<sub>3</sub>(Ce) energy gate on the depopulating 405-keV transition. The measured centroids for the determination of one Compton background component of the lifetime measurement are shown in green and the corresponding polynomial fit in red. The centroid of the shown background component has a value of -74(13) ps. (b) Same coincidence spectra with a LaBr<sub>3</sub>(Ce) energy gate on the populating 223-keV transition. It is also shown the polynomial fit, which provides the centroid of this background component by a value of -79(15) ps. (c) Raw time difference distribution obtained with a LaBr<sub>3</sub>(Ce) coincidence gate on the 223-keV and 405-keV transition. The measured centroid position is shown in orange.

$C^P(223 \text{ keV}, 405 \text{ keV}) = -7(7) \text{ ps}$ , taken from the time walk curve in Fig. 2, the resulting mean lifetime is given by

$$\tau_{4_1^+} = 100(14) \text{ ps.}$$

A SLTD gate on the *prompt region* yields the same result but with larger systematic uncertainty due to the larger amount of contaminations and the poorer peak-to-background ratio (0.50(2) for the 223-keV peak and 0.61(2) for the 405-keV peak), which made the uncertainty of the lifetime too large for a precise determination.

Additionally to check the analysis, the mean lifetime of the  $2_1^+$  state was determined. The resulting value (16(13) ps) is compatible with the previously reported lifetime value (20.5(26) ps [8]). The lifetime of the  $4_1^+$  state is also determined indirectly by the time difference distribution gated on the coincidence transitions

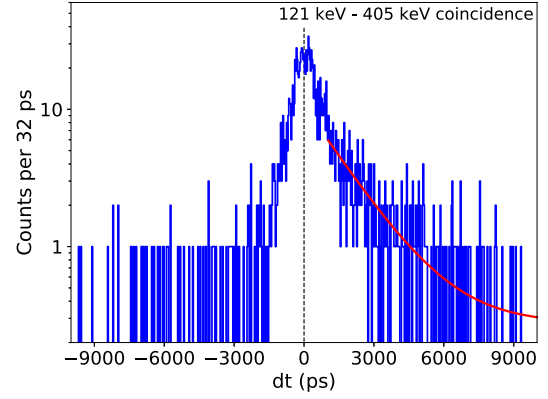


**Fig. 6.** Raw time difference distribution obtained with a LaBr<sub>3</sub>(Ce) coincidence gate on the 121-keV and 405-keV transition. In red is shown the slope fit with a constant to approximate the random background.

223 keV and 727 keV. The centroid position  $C$  of this distribution is shifted by the sum of the lifetimes of the intermediate states [20]:

$$C(223 \text{ keV}, 727 \text{ keV}) = C^P(223 \text{ keV}, 727 \text{ keV}) + \tau_{2_1^+} + \tau_{4_1^+}.$$

The measured sum of both lifetimes (114(18) ps) indicates the same mean lifetime for the  $4_1^+$  state and confirmed the measured mean lifetime using the 223 keV - 405 keV coincidence.

### 3.3. Lifetime determination of the $6_1^+$ state

Only one experimental value for the  $6^+$  state lifetime has been published by A. Poletti et al. [16]. They report a value of 1.1(3) ns. The main experimental challenge of the lifetime determination of this state is the low energy E2-transition populating the  $6_1^+$  state (121 keV) and the associated strong internal electron conversion coefficient (3.24(5) [27]). Therefore, the  $\gamma$ -ray statistics for analysing this state are much lower than the statistics for the determination the lifetime of the  $4_1^+$  state, but the peak is clearly visible in the coincidence spectrum of the 405-keV transition in Fig. 5(a).

The time difference distribution of the 121 keV - 405 keV coincidence is shown in Fig. 6. Due to the peak-to-background ratio of the 121-keV peak (0.39(5)) and 405-keV peak (0.51(5)) in the coincidence spectra, the spectrum is dominated by the prompt background distribution. However the comparatively long lifetime of the  $6_1^+$  state is well visible by the slope to positive time differences. The lifetime is determined by the slope method (1.75(26) ns) and centroid shift method (1.56(30) ns). The average mean lifetime has a value of

$$\tau_{6_1^+} = 1.66(28) \text{ ns.}$$

This mean lifetime is larger than the current literature value (1.1(3) ns [16]) but it has to be mentioned that the lifetime of the  $6_1^+$  state in Ref. [16] depends by the lifetime of the  $8_1^+$  state which is in Ref. [16] (24.6(3) ns) longer compared to the lifetime determined by three other measurements (20.2(14) ns [7], 20.5(35) ns [14], 21.2(4) ns [15]) and this work (20.8(17) ns).

## 4. Discussion

Taking into account the newly derived lifetime of the  $4_1^+$  state (100(14) ps), the internal electron conversion coefficient for the  $4_1^+ \rightarrow 2_1^+$  transition of  $^{212}\text{Po}$  (0.0544(8) [27]) and the  $\alpha$ -branching

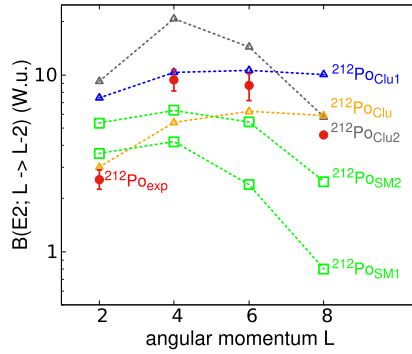


**Fig. 7.** Semi logarithmic plot of the  $B(E2)$  transition strength for the low-lying yrast states of  $^{212}\text{Po}$ . The experimental values (from Ref. [10] and this analysis) are marked in red. The theoretical values of  $^{212}\text{Po}$  come from shell-model approaches (SM1 from Ref. [8] and SM2 from Ref. [11]), and from  $\alpha$ -clustering models (Clu1 from Ref. [4], Clu2 from Ref. [9] and Clu are the calculations from this work).

ratio of 0.5% [7,10], the missing absolute transition strength is given by

$$B(E2; 4_1^+ \rightarrow 2_1^+) = 9.4(13) \text{ W.u.}$$

It is worth to mention that the statements of Ref. [7] regarding the  $\alpha$ -branching ratio of 27% [13] and the smaller ratio were confirmed within this analysis. We have applied the same method as in Ref. [7] by setting a gate on a coincidence transition above the feeding transition and taking the relative intensity in the coincidence spectrum between the transition feeding the state of interest and transitions below this state. The relative intensities between the 223-keV transition and the 405-keV and 727-keV transition in the HPGe coincidence spectra are 1.01(8) and 0.98(10) respectively.

Due to the larger lifetime of the  $6_1^+$  state (1.66(28) ns), the internal electron conversion coefficient of the  $6_1^+ \rightarrow 4_1^+$  transition (0.324(5) [27]) and  $\alpha$ -branching ratio of 3% [10], the  $B(E2; 6_1^+ \rightarrow 4_1^+)$  value decreases to 8.7(15) W.u. It was tried to check the  $\alpha$ -branching ratio of the  $6_1^+$  state with the isomeric SLTD gate and the resulting LaBr<sub>3</sub>(Ce) single spectrum, but the contaminations by  $^{212}\text{At}$  and another transitions are too strong for a quantitative statement about this ratio based on data from this work.

During the present work, a new  $\alpha$ -clustering calculation has been performed in the frame of the Dinuclear System Model (DNS) [28]. The model is based on the assumption that the cluster-type shapes are produced by the motion of the nucleus in the mass asymmetry degree of freedom  $\xi$ . The nuclear wave function is treated as a superposition of mononucleus (spherical in the case of  $^{212}\text{Po}$ ) and cluster configurations. The weights of various components are determined by the solution of the Schrödinger equation with Hamiltonian in mass asymmetry (Ref. [29])

$$H(I) = -\frac{\hbar^2}{2B} \frac{1}{\xi} \frac{\partial}{\partial \xi} \xi \frac{\partial}{\partial \xi} + U(\xi, I), \quad (1)$$

where  $B$  is the mass parameter and  $U(\xi, I)$  is the potential energy in mass asymmetry for a given angular momentum  $I = 0, 2, 4, \dots$ . The members of the ground-state band are described as the lowest eigenfunctions of  $H(I)$ .

The energies of cluster configurations are calculated as a sum of the binding energies of corresponding fragments and nucleus-nucleus potential. The details of calculations are presented in Ref. [29]. The energy of the mononucleus configuration cannot be determined within the DNS model. Since, for  $^{212}\text{Po}$ , we deal with two protons and two neutrons outside a spherical double magic core, the structure of the mononucleus is mainly determined by the shell model configuration with two neutrons and two protons in the  $2g_{9/2}$  and  $1h_{9/2}$  shell, respectively, [8]. This leads to the

**Table 1**

$B(E2)$  values and  $\alpha$ -branching ratios from the low-lying yrast states. The theoretical values are calculated in the  $\alpha$ -clustering model from the present work. The experimental  $B(E2)$  values are taken from this analysis and from Ref. [10].

State I	$B(E2; I \rightarrow I-2)$		$\alpha$ -branching ratios		
	exp. (W.u.)	theo. (W.u.)	Ref. [10] (%)	Ref. [13] (%)	theo. (%)
$2_1^+$	2.6(3)	3.01	0.033	0.033	0.18
$4_1^+$	9.4(13)	5.39	$\sim 0.5$	27	3.92
$6_1^+$	8.7(15)	6.23	$\sim 3$	71	15.20
$8_1^+$	4.6(1)	5.90	$\sim 3$	42	7.71

seniority-like spectrum up to  $I = 8$ , where the onset of  $2p2h$  components breaks the smooth variation of the excitation spectrum with  $I$ . The energies of the yrast states of  $^{212}\text{Po}$  are mainly determined by the mononucleus configuration, since its weight is much larger than that of the cluster components (see Table 2). Therefore, the pattern of the excitation spectrum of  $^{212}\text{Po}$  largely corresponds to the behavior of the mononucleus spectrum. However, for the description of  $B(E2)$ 's the weight of the cluster components is of crucial importance because of the large (collective) value of the quadrupole transitional moment for the cluster configurations. Since in this work we are interested in the calculation of  $B(E2)$  values and lifetimes of the yrast states in  $^{212}\text{Po}$ , the energy of the mononucleus configuration was not calculated, instead it was fitted to describe the experimental energy  $E_{exp}(I)$  as the lowest eigenvalue of (1).

Our calculations show that for the DNS's with light clusters heavier than an  $\alpha$ -particle, the potential energy rapidly increases. Therefore, the mononucleus configuration and  $\alpha$ -particle DNS are the only components contributing significantly to the wave functions of yrast states in  $^{212}\text{Po}$ . The weights of these components and their change with angular momentum are determined by the difference  $\Delta E(I) = E_\alpha(I) - E_m(I)$  between the potential energies of  $\alpha$ -cluster DNS and the mononucleus. The lower  $U(I)$  for the  $\alpha$ -particle system is with respect to the mononucleus, the higher its weight, and vice versa.

As found, the energy of  $\alpha$ -cluster DNS at  $I = 0$  is 1.8 MeV higher than the binding energy of  $^{212}\text{Po}$ . It increases with angular momentum according to rotational law. The moment of inertia of  $\alpha$ -cluster DNS is calculated within the cranking approximation using the wave function of two-center shell model [30]. This moment of inertia is about 30% of the corresponding rigid body value. Alternatively, the spectrum of the mononucleus behaves like in the pairing-coupling scheme. It shows strongly bound  $I = 0$  state while the increase rate of energies of states with higher angular momenta slows down with  $I$  up to  $I = 8$ .

As a result of different behavior of energies of  $\alpha$ -cluster DNS and mononucleus with angular momentum, we observe that  $\Delta E(I)$  first fastly decreases up to  $I = 4$  and then increases up to  $I = 8$ . The weight of the  $\alpha$ -cluster system calculated as

$$\omega_I = \int_{\xi_\alpha/2}^{\infty} |\Psi_I(\xi)|^2 \xi d\xi \quad (2)$$

increases strongly for  $I = 2$  and  $I = 4$  states and then slowly decreases. Here,  $\xi_\alpha$  is the mass asymmetry value corresponding to the  $\alpha$ -cluster DNS. Results are presented in Table 2.

The reduced probabilities of  $E2$  transitions are calculated as

$$B(E2, I_i \rightarrow I_f) = \frac{5}{4\pi} \left( C_{I_i 0 20}^{I_f 0} \int_0^{\infty} \Psi_{I_f}(\xi) q_0(\xi) \Psi_{I_i}(\xi) \xi d\xi \right)^2, \quad (3)$$

**Table 2**

Weights of alpha-particle cluster system and the width of alpha-decay  $\Gamma_\alpha$  calculated in the  $\alpha$ -clustering model from the present work.

State $l$	$\omega_l$	$\Gamma_\alpha(I)/\hbar$ in $s^{-1}$
$0_1^+$	0.116	$2.36 \cdot 10^6$
$2_1^+$	0.170	$1.02 \cdot 10^8$
$4_1^+$	0.199	$2.32 \cdot 10^8$
$6_1^+$	0.190	$7.49 \cdot 10^7$
$8_1^+$	0.158	$4.99 \cdot 10^6$

where the transition operator is

$$q_0(\xi) = e_2 \frac{A_1^2 Z_2 + A_2^2 Z_1}{A^2} R^2. \quad (4)$$

Here  $A_i(Z_i)$ , ( $i = 1, 2$ ) are the masses (charges) of clusters and  $R$ -distance between the centers of the clusters. The effective charge for the quadrupole transition is taken as  $e_2 = 1$ .

The calculated  $B(E2)$  transition strengths are shown in Fig. 7 and listed in Table 1. The experimental  $B(E2; 2_1^+ \rightarrow 0_1^+)$  value is well predicted by this calculation. In contrast to the shell-model calculations, an enhancement of the  $B(E2)$  values for the decay from the  $4_1^+$ ,  $6_1^+$  and  $8_1^+$  state is also described. As seen from (4), the strength of quadrupole transitions is wholly determined by the weight of the  $\alpha$ -cluster component in the wave functions. The strong increase of  $\alpha$ -particle weight at  $l = 2$  allows us to understand the enhancement of  $B(E2)$  values.

The absolute values of  $B(E2; 4_1^+ \rightarrow 2_1^+)$  and  $B(E2; 6_1^+ \rightarrow 4_1^+)$  are somewhat underestimated in the present calculation. Also, the experimental trend shows the decrease of  $B(E2, I \rightarrow I - 2)$  values after  $l = 4$ , while in the DNS model the decrease starts from  $l = 6$ . This trend is better described by  $\alpha$ -clustering model calculation from Ref. [9] but the absolute values are most overestimated by this calculation. Overall, cluster models calculations appear to be more appropriate than the current shell-model predictions.

Using the calculated weights, we obtain the decay width  $\Gamma_\alpha(I)$  of  $\alpha$  decay in WKB approximation (Ref. [31]). The results are presented in Table 2. To obtain more accurate angular momentum dependence of  $\Gamma_\alpha(I)$ , the frequency of the barrier assaults is fixed to reproduce the  $\alpha$ -decay half-life of the ground-state of  $^{212}\text{Po}$ :  $\hbar\nu_0 = 1.35$  MeV. This value is comparable with  $\hbar\nu_0 = 1.2$  MeV taken in Ref. [31].

Using the calculated  $\Gamma_\alpha(I)$  and  $B(E2, I \rightarrow I - 2)$  values, we obtain the  $\alpha$ -branching ratios presented in Table 1. The theoretically calculated  $\alpha$ -branching ratios are closer to the experimental branching reported in Ref. [10] and are significantly lower than the ones reported in Ref. [13].

## 5. Conclusion

In this work we have measured the lifetime of the low-lying yrast states of  $^{212}\text{Po}$  by utilizing different fast-timing techniques. A very important feature of the analysis was the first combination between a fast-timing measurement and a particle detector setup to investigate states below an isomer. The results are shown in Table 3. The lifetime of the  $4_1^+$  state is determined for the first time in this work.

The extracted  $B(E2; 4_1^+ \rightarrow 2_1^+) = 9.4(13)$  W.u. value completes the experimental dataset of the low-lying yrast states. This electromagnetic transition strength and the new derived  $B(E2; 6_1^+ \rightarrow 4_1^+) = 8.7(15)$  W.u. value are an important contribution to the knowledge about the nuclear structure of  $^{212}\text{Po}$ . The available experimental data on the electromagnetic transition strengths for the yrast states in  $^{212}\text{Po}$  is adequately described, at least qualitatively,

**Table 3**

Measured mean lifetimes  $\tau$  of the low-lying yrast states of  $^{212}\text{Po}$  resulting from the presented analysis. The literature mean lifetimes are taken from Ref. [10].

State	This work	Literature
$2_1^+$	16(13) ps	20.5(26) ps
$4_1^+$	100(14) ps	-
$6_1^+$	1.66(28) ns	1.1(3) ns
$8_1^+$	20.8(17) ns	21.1(4) ns

in the framework of an  $\alpha$ -clustering model. This suggests that  $\alpha$ -cluster components play an important role in the structures of these states. To fully prove this conjecture more experimental information on the  $\alpha$ -branchings and the static electromagnetic moments of the yrast states in  $^{212}\text{Po}$  is needed.

## Declaration of competing interest

The authors declare that they have no known competing financial interests or personal relationships that could have appeared to influence the work reported in this paper.

## Acknowledgements

Funding support is acknowledged from the EURONS2, IFA via grant 04FAIR/2020 and MCDI via grant PN19060102. KRM, MS, PS, acknowledge financial support by the UK-STFC via grant ST/P005101/1. T.M.S. was partly supported by the Ministry of Science and Higher Education of the Russian Federation (Moscow, Contract No. 075-10-2020-117).

We especially thank the accelerator group of the Bucharest FN Tandem Accelerator and the local people of IFIN (HH) for their hospitality during the experimental campaign.

## References

- [1] M.G. Mayer, Nuclear configurations in the spin-orbit coupling model. I. Empirical evidence, *Phys. Rev.* 78 (1950) 16–21, <https://doi.org/10.1103/PhysRev.78.16>.
- [2] C. Qi, A.N. Andreyev, M. Huysse, R.J. Liotta, P. Van Duppen, R.A. Wyss, Abrupt changes in  $\alpha$ -decay systematics as a manifestation of collective nuclear modes, *Phys. Rev. C* 81 (2010) 064319, <https://doi.org/10.1103/PhysRevC.81.064319>.
- [3] K. Varga, R.G. Lovas, R.J. Liotta, Absolute alpha decay width of  $^{212}\text{Po}$  in a combined shell and cluster model, *Phys. Rev. Lett.* 69 (1992) 37–40, <https://doi.org/10.1103/PhysRevLett.69.37>.
- [4] F. Hoyle, P. Mohr, G. Staudt, Alpha-cluster states of  $^{212}\text{Po}$  in a realistic potential model, *Phys. Rev. C* 50 (1994) 2631–2634, <https://doi.org/10.1103/PhysRevC.50.2631>.
- [5] B. Buck, J.C. Johnston, A.C. Merchant, S.M. Perez, Cluster model of  $\alpha$  decay and  $^{212}\text{Po}$ , *Phys. Rev. C* 53 (1996) 2841–2848, <https://doi.org/10.1103/PhysRevC.53.2841>.
- [6] A. Astier, P. Petkov, M.-G. Porquet, D.S. Delion, P. Schuck, Novel manifestation of  $\alpha$ -clustering structures: new “ $\alpha + ^{208}\text{Pb}$ ” states in  $^{212}\text{Po}$  revealed by their enhanced  $e1$  decays, *Phys. Rev. Lett.* 104 (2010) 042701, <https://doi.org/10.1103/PhysRevLett.104.042701>.
- [7] A. Astier, P. Petkov, M.-G. Porquet, D.S. Delion, P. Schuck, Coexistence of “ $\alpha + ^{208}\text{Pb}$ ” cluster structures and single-particle excitations in  $^{212}\text{Po}$ , *Eur. Phys. J. A* 46 (2010) 165–185, <https://doi.org/10.1140/epja/i2010-11053-6>.
- [8] D. Kocheva, G. Rainovski, J. Jolie, N. Pietralla, A. Blazhev, et al., Low collectivity of the  $2_1^+$  state of  $^{212}\text{Po}$ , *Phys. Rev. C* 96 (2017) 044305, <https://doi.org/10.1103/PhysRevC.96.044305>.
- [9] D.S. Delion, R.J. Liotta, P. Schuck, A. Astier, M.-G. Porquet, Shell model plus cluster description of negative parity states in  $^{212}\text{Po}$ , *Phys. Rev. C* 85 (2012) 064306, <https://doi.org/10.1103/PhysRevC.85.064306>.
- [10] K. Auranen, E. McCutchan, Nuclear data sheets for  $A=212$ , *Nucl. Data Sheets* 168 (2020) 117–267, <https://doi.org/10.1016/j.nds.2020.09.002>.
- [11] H. Naidja, New shell-model investigation of the lead-208 mass region: spectroscopic properties and collectivity, *Phys. Rev. C* 103 (2021) 054303, <https://doi.org/10.1103/PhysRevC.103.054303>.
- [12] K. Eskola, P. Eskola, M.M. Fowler, H. Ohm, E.N. Treher, J.B. Wilhelmy, D. Lee, G.T. Seaborg, Production of neutron-rich Bi isotopes by transfer reactions, *Phys. Rev. C* 29 (1984) 2160–2168, <https://doi.org/10.1103/PhysRevC.29.2160>.

- [13] E. Browne, Nuclear data sheets for  $A = 212$ , Nucl. Data Sheets 104 (2005) 427–496, <https://doi.org/10.1016/j.nds.2005.01.002>.
- [14] R.M. Lieder, J.P. Didelez, H. Beuscher, D.R. Haenni, M. Müller-Veggian, A. Neskakis, C. Mayer-Böricke, Observation of a new isomer in  $^{212}\text{Po}$ , Phys. Rev. Lett. 41 (1978) 742–745, <https://doi.org/10.1103/PhysRevLett.41.742>.
- [15] H. Bohn, E. Endres, T. Faestermann, P. Kienle, Spectroscopy of excited states in  $^{212}\text{Po}$ ,  $^{210}\text{Pb}$ , and  $^{213}\text{At}$  employing  $^{18}\text{O}$  induced few-nucleon transfer reactions, Z. Phys. A 302 (1981) 51, <https://doi.org/10.1007/BF01425102>.
- [16] A. Poletti, G. Dracoulis, A. Byrne, A. Stuchbery, The low-lying yrast structure of  $^{212}\text{Po}$ , Nucl. Phys. A 473 (3) (1987) 595–604, [https://doi.org/10.1016/0375-9474\(87\)90141-2](https://doi.org/10.1016/0375-9474(87)90141-2).
- [17] S. Dobrescu, D.V. Mosu, D. Moisa, S. Papureanu, The BucharestFN tandem accelerator: modernization and development, AIP Conf. Proc. 1099 (1) (2009) 51–54, <https://doi.org/10.1063/1.3120087>.
- [18] D. Bucurescu, et al., The rosphere  $\gamma$ -ray spectroscopy array, Nucl. Instrum. Methods Phys. Res., Sect. A, Accel. Spectrom. Detect. Assoc. Equip. 837 (2016) 1–10, <https://doi.org/10.1016/j.nima.2016.08.052>.
- [19] T. Beck, et al., Sorcerer: a novel particle-detection system for transfer-reaction experiments at rosphere, Nucl. Instrum. Methods Phys. Res., Sect. A, Accel. Spectrom. Detect. Assoc. Equip. 951 (2020) 163090, <https://doi.org/10.1016/j.nima.2019.163090>.
- [20] H. Mach, R. Gill, M. Moszyński, A method for picosecond lifetime measurements for neutron-rich nuclei: (1) outline of the method, Nucl. Instrum. Methods Phys. Res., Sect. A, Accel. Spectrom. Detect. Assoc. Equip. 280 (1) (1989) 49–72, [https://doi.org/10.1016/0168-9002\(89\)91272-2](https://doi.org/10.1016/0168-9002(89)91272-2).
- [21] J.-M. Régis, G. Pascovici, J. Jolie, M. Rudigier, The mirror symmetric centroid difference method for picosecond lifetime measurements via  $\gamma$ - $\gamma$  coincidences using very fast  $\text{LaBr}_3(\text{Ce})$  scintillator detectors, Nucl. Instrum. Methods Phys. Res., Sect. A, Accel. Spectrom. Detect. Assoc. Equip. 622 (1) (2010) 83–92, <https://doi.org/10.1016/j.nima.2010.07.047>.
- [22] NNDC, <https://www.nndc.bnl.gov/ensdf>, 2021. (Accessed 1 July 2021).
- [23] J.-M. Régis, A. Esmaylzadeh, J. Jolie, V. Karayonchev, L. Knafla, U. Köster, Y. Kim, E. Strub,  $\gamma$ - $\gamma$  fast timing at x-ray energies and investigation on various timing deviations, Nucl. Instrum. Methods Phys. Res., Sect. A, Accel. Spectrom. Detect. Assoc. Equip. 955 (2020) 163258, <https://doi.org/10.1016/j.nima.2019.163258>.
- [24] S. Ilieva, T. Kröll, J.-M. Régis, N. Saed-Samii, et al., Measurement of picosecond lifetimes in neutron-rich Xe isotopes, Phys. Rev. C 94 (2016) 034302, <https://doi.org/10.1103/PhysRevC.94.034302>.
- [25] S. Ansari, J.-M. Régis, J. Jolie, N. Saed-Samii, N. Warr, W. Korten, M. Zielińska, M.-D. Salsac, et al., Experimental study of the lifetime and phase transition in neutron-rich  $^{98,100,102}\text{Zr}$ , Phys. Rev. C 96 (2017) 054323, <https://doi.org/10.1103/PhysRevC.96.054323>.
- [26] A. Esmaylzadeh, L.M. Gerhard, V. Karayonchev, J.-M. Régis, J. Jolie, et al., Lifetime determination in  $^{190,192,194,196}\text{Hg}$  via  $\gamma$ - $\gamma$  fast-timing spectroscopy, Phys. Rev. C 98 (2018) 014313, <https://doi.org/10.1103/PhysRevC.98.014313>.
- [27] Bricc, Band-Raman internal conversion coefficients, <https://bricc.anu.edu.au/>, 2021. (Accessed 29 May 2021).
- [28] T.M. Shneidman, G.G. Adamian, N.V. Antonenko, R.V. Jolos, W. Scheid, Cluster interpretation of properties of alternating parity bands in heavy nuclei, Phys. Rev. C 67 (2003) 014313, <https://doi.org/10.1103/PhysRevC.67.014313>.
- [29] T.M. Shneidman, G.G. Adamian, N.V. Antonenko, R.V. Jolos, S.-G. Zhou, Cluster approach to the structure of  $^{240}\text{Pu}$ , Phys. Rev. C 92 (2015) 034302, <https://doi.org/10.1103/PhysRevC.92.034302>.
- [30] J. Maruhn, W. Greiner, The asymmetrie two center shell model, Z. Phys. A 251 (1972) 431.
- [31] S.N. Kuklin, G.G. Adamian, N.V. Antonenko, Spectroscopic factors and cluster decay half-lives of heavy nuclei, Phys. Rev. C 71 (2005) 014301, <https://doi.org/10.1103/PhysRevC.71.014301>, <https://link.aps.org/doi/10.1103/PhysRevC.71.014301>.